DNA AND CELL BIOLOGY
Volume 29, Number 3, 2010

Pp. 149–160
DOI: 10.1089/dna.2009.0858

# Mass Spectroscopy and Molecular Modeling Predict Endothelial Nitric Oxide Synthase Dimer Collapse by Hydrogen Peroxide Through Zinc Tetrathiolate Metal-Binding Site Disruption

Fabio V. Fonseca,[1] Kandasamy Ravi,[2] Dean Wiseman,[1] Monorama Tummala,[3] Cynthia Harmon,[4] Victor Ryzhov,[3] Jeffrey R. Fineman,[4,5] and Stephen M. Black[1]

Endothelial nitric oxide synthase (eNOS) is inhibited by hydrogen peroxide ($H_2O_2$), but the mechanism has not been determined. Thus, the purpose of this study was to delineate the mechanism by which $H_2O_2$ inhibits eNOS activity. Using mass spectroscopy, we found that the tetrathiolate cysteine residues 94 and 99 were susceptible to oxidation by $H_2O_2$. Molecular modeling predicted that these cysteic acid modifications would disrupt the van der Waals interactions and the hydrogen bonding network mediated by the tetrathiolate cysteines 94 and 99 resulting in changes in quaternary structure, zinc release, and dimer collapse. Using recombinant human eNOS (heNOS) to test the predictions of the molecular modeling we found that $H_2O_2$ caused disruption of the heNOS dimer and this was accompanied by zinc release and decreased NO generation. We also found that $H_2O_2$ increased the oxidation of tetrahydrobiopterin ($BH_4$) to dihydrobiopterin ($BH_2$), whereas preincubation of heNOS with excess $BH_4$ prevented the destruction of zinc tetrathiolate and dimer collapse and preserved activity. Interestingly, we found that the dimmer-stabilizing effect of $BH_4$ is due to its ability to act as a catalase mimetic. Further, we confirmed that, in ovine aortic endothelial cells, $H_2O_2$ could also induce dimer collapse and that increasing cellular $BH_4$ levels could maintain eNOS in its dimeric form and NO signaling when cells were challenged with $H_2O_2$. This study links the inhibitory action of $H_2O_2$ on heNOS through the destruction of zinc tetrathiolate metal-binding site and dimer collapse both *in vitro* and *in vivo*.

## Introduction

Vascular endothelial cells produce nitric oxide (NO), which is an important signaling molecule in the regulation of vascular tone and platelet aggregation. NO is synthesized as a by-product during oxidation of L-arginine to L-citrulline by the enzyme NO synthase (NOS). Three isoforms of NOS exist, two constitutively active forms are found in endothelial cells (eNOS) and neurons (nNOS) and an inducible form is found in macrophages (iNOS). NO is a major endothelium-derived relaxing factor of the arterial circulation. Thus any perturbation on the synthesis of NO can have significant effects on blood pressure, flow, and vascular resistance (Knowles, 1996).

Endothelial dysfunction is a hallmark of many diseases of the vasculature including pulmonary and systemic hypertension, atherosclerosis, and diabetes (Griendling *et al.*, 2000a, 2000b). Oxidative stress and reactive oxygen species (ROS) are thought to play a major role in the development of endothelial dysfunction (Lubos *et al.*, 2008; Munzel *et al.*, 2008). Hydrogen peroxide ($H_2O_2$) is a nonradical ROS that can contribute to overall oxidative stress. It is primarily produced from superoxide anion by superoxide dismutase. Among all ROS species, $H_2O_2$ presents the lowest reduction potential, greatest half-life, and highest intracellular concentration and does not react with NO (Giorgio *et al.*, 2007). $H_2O_2$ is a membrane-permeable molecule that can act as a signaling molecule because of its intrinsic ability to induce fully reversible protein modifications. $H_2O_2$ can directly oxidize cysteine residues to sulphenic acids and induce glutathionylation of cysteine residues or sulphoxidation of methionine residues in several cellular targets (Forman *et al.*, 2004). Previous studies indicate that exogenous NO exposure inhibits eNOS activity (Sheehy *et al.*, 1998; Black *et al.*, 1999). The molecular mechanism proposed was through S-nitrosylation of cysteines 94 and 99. This modification causes the disruption of zinc tetrathiolate

[1]Vascular Biology Center, Medical College of Georgia, Augusta, Georgia.
[2]Cold Spring Harbor Laboratories, Cold Spring Harbor, New York.
[3]Department of Chemistry and Biochemistry, Northern Illinois University, DeKalb, Illinois.
Departments of [4]Pediatrics and [5]Cardiovascular Research Institute, University of California, San Francisco, California.

metal-binding site, dimer collapse, and loss of enzymatic activity (Ravi *et al.*, 2004). In addition, it has been demonstrated that increases in intracellular $H_2O_2$ concentration induced by nicotinamide adenine dinucleotide phosphate (NADPH) oxidase activation can inhibit both eNOS expression and activity (Wedgwood and Black, 2005). Based on all these data, we hypothesized that molecular mechanism by which $H_2O_2$ inhibits eNOS activity could involve, at least in part, dimer collapse.

In this study, we investigated the molecular effects on eNOS activity and dimeric structure, through a model of an acute oxidant stress exerted by $H_2O_2$ challenge. Our results describe, for the first time, that this inhibitory phenomenon involves the oxidation of tetrahydrobiopterin ($BH_4$) and cysteine residues 94 and 99 within the zinc metal-binding site of eNOS. These oxidative reactions lead to eNOS dimer collapse, zinc release, and impairment of NO generation both *in vitro* and *in vivo*. Our data also suggest that $BH_4$, by virtue of its antioxidant capacity, prevents the oxidation of the zinc tetrathiolate metal-binding site and maintains the eNOS dimer. We speculate that eNOS monomerization may be a general inhibitory mechanism in conditions of high oxidative and nitrosative stress.

## Materials and Methods

### Chemicals

L-Arginine, flavin adenine dinucleotide (FAD), NADPH, calmodulin, Dowex 50W-X8, phenyl methyl sulfonyl fluoride, pepstatin A, leupeptin, protease inhibitor cocktail, 4-(2-pyridyl (azo) resorcinol) (PAR), standard molecular weight markers for gel filtration, *S*-nitroso *N*-acetyl penicillamine, *N*-acetyl penicillamine, ethylenediaminetetraacetic acid, and ethylene glycol tetraacetic acid (EGTA) were purchased from Sigma (St. Louis, MO); Ni-NTA resin from Novagen (Carlsbad, CA); calmodulin sepharose, adenosine diphosphate (ADP)-sepharose, and L-[2,3,4,5-3H] arginine from Amersham-Pharmacia Biotech (Piscataway, NJ); monoclonal antibodies against eNOS from Transduction Laboratories (Franklin Lakes, NJ); Luria Broth (LB) and Scintiverse II from Fisher (Pittsburg, PA); Isopropyl β-D-1-thiogalactopyranoside (IPTG) from Life Technologies (Carlsbad, CA); BL21(DE3)-pLysS from Novagen; western blotting and Coomassie staining reagents from Pierce (Rockford, IL); BioSpin P-30 Tris columns from BioRad (Hercules, CA); modified trypsin from Promega (Madison, WI); and disposable minicolumns, Chelex-100, and Bradford reagent for protein determination from BioRad. The poly-His-pCWeNOS vector was a gift from P.R. Ortiz de Montellano (University of California, San Francisco). $BH_4$ was obtained from Schirck's Lab (Jona, Switzerland), and unless otherwise mentioned all other chemicals were purchased from Sigma.

### Expression and purification of wild-type human eNOS

Protein expression and purification were performed as previously described by Ravi *et al.* (2004). The recombinant human eNOS (heNOS) protein was purified to 95% with a yield of $\sim$20–30 mg/8 L of culture.

### Oxidation with $H_2O_2$ and proteolytic digest of recombinant heNOS

One hundred microliters of heNOS ($\sim$0.8 μg/μL) was passed through a BioSpin column preequilibrated with HEN buffer (250 mM HEPES [pH 7.7], 1 mM ethylenediaminetetraacetic acid, 0.1 mM neocuproine) to remove dithiotlreitol (DTT). Zinc was added to the protein in the molar ratio of 2:1 (protein:Zn). Then $H_2O_2$ was added to bring the final concentration to 50 μM and incubated for 30 min at 37°C. The sample was centrifuged again with Biospin column to remove excess peroxide and 200 μL of 8 M urea and 0.4 M ammonium bicarbonate (pH 7.5) were added. To reduce the disulfide bonds, 50 μL of 45 mM DTT was added to the sample and incubated at 50°C for 15 min. After bringing the sample to room temperature, 50 μL of 100 mM iodoacetamide was added and left in the dark for 15 min. The sample was diluted to 2 M urea and 0.1 M ammonium bicarbonate by adding water. Twenty microliters of trypsin (0.1 μg/μL) was added and incubated at 37°C overnight. Digestion was stopped by freezing and then the sample was lyophilized. For subsequent AspN protease digest, 20 μL of 15 ng/μL AspN in 50 mM ammonium bicarbonate was added to the sample after resuspending the sample in 100 μL of 50 mM ammonium bicarbonate buffer. The sample was left to digest overnight at 37°C. The digest was dried and resuspended in water for mass spectral analysis.

### Nano-liquid chromatography–mass spectroscopy/mass spectroscopic analysis

Samples were desalted online on a $C_{18}$ trap and then eluted across a $C_{18}$ column into the mass spectrometer. The samples were desalted for 10 min with 100% solvent A and then turned to next column at gradient of 5–60% solvent B for 40 min. Solvent A consisted of 100% water with 0.1% formic acid, and solvent B was 80% acetonitrile (ACN) and 0.1% formic acid in water. Flow rate was 250 nL/min. ThermoElectron LTQ linear ion trap mass spectrometer (ThermoElectron, San Jose, CA) equipped with a nanospray ionization source with a 10 cm$\times$75 μm $C_{18}$-packed nanospray tip was used. The stationary phase was Biobasic $C_{18}$, 3-μm particles.

### Molecular modeling

The zinc tetrathiolate coordination model was obtained using the Discovery Studio (DS) 2.1 (Accelrys, San Diego, CA) software package. Van der Waals interactions and hydrogen bonds (H-bonds) were measured. The three-dimensional crystallographic structure of eNOS was obtained from the Research Collaboratory for Structural Bioinformatics (RCSB) protein data bank (PDB) accession code 3NOS (human dimeric eNOS with arginine substrate, oxidoreductase domain chains A and B) (Fischmann *et al.*, 1999). The Ramachandran imperfections and missing loops were fixed using Modeller Prepare Protein 37 from DS 2.1. This function prepares any given protein for molecular simulations. This function is composed of five steps: (1) build loops (type = BoolType) that determine if missing loops are being inserted based on SEQRES data; (2) use looper; (3) use modeller; (4) use CHARMm minimization, and (5) use maximal loop length. The maximal loop length step used was of long type. The prepare protein of DS 2.1 also has a protonate step that determines whether or not to protonate the final structure with the protein ionization method. The protonation is based on protein dielectric constant analysis and calculations of pH for protonation. The protein dielectric constant specifies the dielectric constant of the protein interior. The function pH for protonation specifies the proper pH value

to protonate the molecule. The force field utilized by the prepare protein function was of STRINGTYPE, and this specifies the force field to be used for matrix calculations (CHARMm, CHAMPLR, CHARMm 19, CHARMm 22, and CHARMm 27). In addition, this method also utilizes a prepare protein structure function that cleans up common problems in the input protein structure in preparation for further processing by other protocols. Finally, we submitted the prepared 3NOS PDB file to a standard dynamics simulation cascade. This standard dynamics simulation cascade is composed of six steps: (1) the prepared 3NOS PDB file is typed into the DS 2.1 software using the CHARMm force field; (2) a first step of minimization using steepest descent algorithm, using a total of 5000 steps, root mean square (RMS) gradient of 0.001, and no constraints; (3) followed by a second step of minimization using the adopted basis non relativistic (NR) as an algorithm, using a total of 5000 steps, RMS gradient of 0.001, and no constraints; (4) heating step: parameters are 5000 steps, time step 0.001, initial temperature 50.0°F, target temperature 300.0°F, and no constraints; (5) an equilibration step: parameters are 10,000 steps with a time step of 0.001, target temperature 300.0°F, no constraints, constant pressure: false, PMass = 1000.0, PGamma = 25, and reference pressure 1.0; and finally, (6) a production step consisting of 10,000 steps, time step 0.001, target temperature 300.0°F, temperature coupling decay time = 5.0, no constraints, type = constant volume constant temperature ensemble (NVT), TMass = 1000.0, implicit solvent model = generalized born with simple switching (best algorithm in the world), nonbond list radius = 14, nonbond higher cutoff distance = 12, nonbond lower cutoff distance = 10, electrostatics = spherical cutoff, Kappa = 0.34, order = 4, dynamics integrator = leapfrog verlet, apply SHAKE constraint = false, and random number seed = 314159. Finally, after running the molecular dynamics simulation with CHARMm force field, the H-bonds and Van der Waals interactions were monitored by DS 2.1. This gave us the wild-type (WT) 3NOS PDB file (Fig. 1A) ready for cysteic acid modification. After the last two steps, we performed cysteic acid modification on the tetrathiolate cysteines 94 and 99. We then performed another molecular dynamic simulation on this modified file (using the same parameters described), monitored the H-bonds and Van der Waals interactions by DS 2.1, and generated Figure 1B. This figure illustrates the potential effects of a cysteic acid modification on the $ZnS_4$ center.

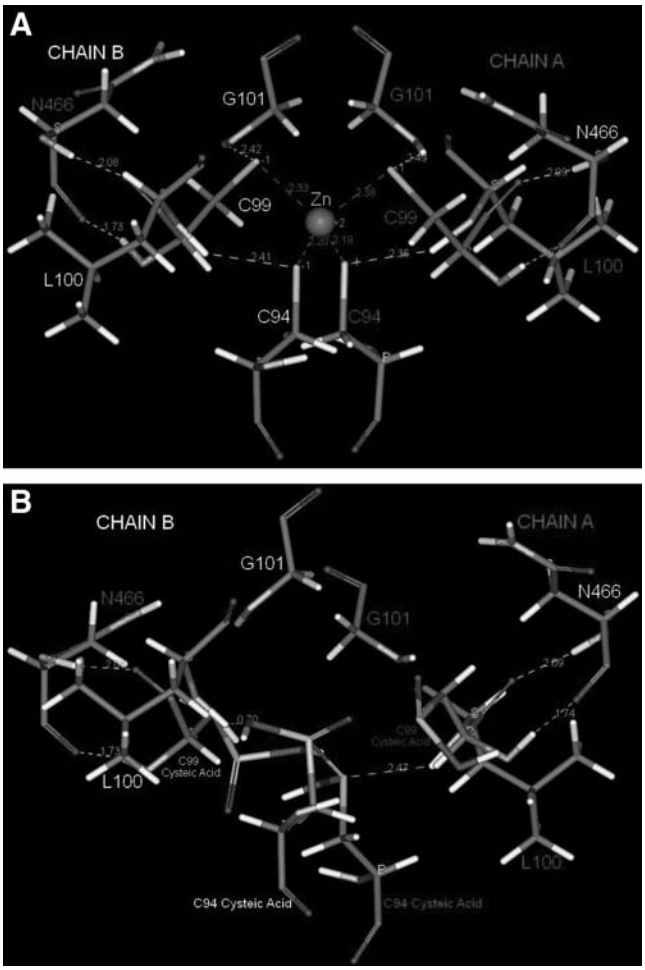


**FIG. 1.** Molecular modeling of the zinc tetrathiolate metal-binding site in heNOS. (**A**) The model shows that cysteines 94 and 99 from each chain are directly involved in four intramolecular van der Waals interactions that are involved in the maintenance of the zinc tetrahedral atomic coordination with the cysteines 94 and 99. The cysteines 94 and 99 also appear to be involved in a network of eight H-bonds with residues N466, G101, and L100. Together these bonds maintain the symmetrical coordination of the C94 and C99 residues. (**B**) The effect of oxidation of cysteines 94 and 99 leading to drastic changes in the quaternary structure of the zinc tetrathiolate coordination due to the disruption of all van der Waals interactions and alterations within the H-bond network. These alterations will disrupt zinc coordination. heNOS, human endothelial nitric oxide synthase.

### *Treatment of purified heNOS with $H_2O_2$*

Fractions of DTT-free purified heNOS (2 μg) were incubated with the reaction mixture containing $H_2O_2$ (0–100 μM) for 30 min at 37°C for the citrulline conversion assay and then the heNOS dimer content was determined using either low-temperature polyacrylamide gel electrophoresis (LT-PAGE) (Ravi *et al.*, 2004) or gel filtration analysis (see below). For gel filtration analysis, 100 μg of DTT-free pure heNOS was incubated with or without $BH_4$ (100 μM) on ice for 1 h, followed by removal of unbound $BH_4$ by buffer exchange (Vivaspin 20 100,000 MWCO PES; Satorius, Goettingen, Germany). heNOS was treated with $H_2O_2$ (100 μM) at 37°C for 30 min, and the dimeric state was analyzed by fast protein liquid chromatography (FPLC), using UV fluorescence detection.

### *Assay for heNOS activity*

This assay was performed by measuring the formation of [$^3$H]citrulline from [$^3$H]arginine, with 10 μM L-arginine as substrate as initially described (Hevel and Marletta, 1994) using our published modifications (Ravi *et al.*, 2004).

### *Zinc release by PAR assay*

Zinc release was measured by PAR assay as initially described (Hevel and Marletta, 1994) using our published modifications (Ravi *et al.*, 2004). All buffers were pretreated with Chelex-100 to remove residual zinc. heNOS was also

purified in buffers treated with Chelex-100. DTT-free purified heNOS protein (1–1.5 mg) was treated with $H_2O_2$ (100 μM) for 30 min in a reaction volume of 200 μL at room temperature in the dark, in the presence or absence of 100 μM $BH_4$. The reaction mixture was added to a cuvette containing 150 μM PAR in 50 mM Tris-Cl and 100 mM NaCl (pH 7.8) in a total volume of 1 mL. The reaction was mixed well and the spectra were recorded from 300 to 600 nm. heNOS protein alone was used to calibrate the spectrophotometer.

### *Quantification of $BH_4$ levels*

DTT-free pure heNOS was preincubated with or without $BH_4$ (50 μM) in ice for 1 h, followed by removal of unbound $BH_4$ by buffer exchange using Centricon. The heNOS protein was treated with $H_2O_2$ (10 μM) at 37°C for 30 min. After this, the spent buffer and the heNOS protein were analyzed for $BH_4$/dihydrobiopterin ($BH_2$) content by HPLC equipped with a fluorescence detector. The HPLC detection was performed using differential oxidation methods of Fukushima and Nixon (1980) using our published modifications (Wainwright *et al.*, 2005).

### *LT-PAGE*

LT-PAGE was carried out according to the procedure of Klatt *et al.* (1995) with our published modification (Ravi *et al.*, 2004). Subsequent to LT-PAGE, gels were transferred to Hybond-ECL nitrocellulose membrane in 20% methanol, 25 mM Tris HCl (pH 8.3), and 192 mM glycine. Western blotting was carried out according to our standard procedures (Hallmark *et al.*, 1999) with mouse anti-eNOS antibody (Transduction Labs). Bands were quantified by densitometric scanning using a Kodak Image station (Carestream Health, Rochester, NY) as previously described (Brennan *et al.*, 2003).

### *Gel filtration chromatography*

Gel filtration chromatography was carried out at 4°C using a Superose 6 HR10/30 column and an FPLC system (Amersham-Pharmacia Biotech). The column was equilibrated with 40 mM 4-(2-hydroxyethyl)-1-piperazinepropanesulfonic acid (EPPS) (pH 7.6), 5% glycerol, and 150 mM NaCl. Typically pure heNOS protein (100 μg) in 200 μL sample volume was injected and the column effluent was monitored at 280 nm using a flow-through UV detector. The column was calibrated with $M_r$ standards: carbonic anhydrase (29 kDa), bovine serum albumin (66 kDa), alcohol dehydrogenase from yeast (150 kDa), α-amylase from sweet potato (200 kDa), apoferritin from horse spleen (443 kDa), and bovine thyroglobulin (669 kDa). The void volume of the column was determined using blue dextran.

### *$H_2O_2$ dismutation assay*

$H_2O_2$ dismutation was determined using a modification of the method of Aebi (1984). To estimate the ability of $BH_4$ to dismutate $H_2O_2$, a solution of 10 mM $H_2O_2$ in 50 mM potassium phosphate buffer (pH 7.8) in the presence or absence of 14 μM of $BH_4$ was analyzed for the disappearance of $H_2O_2$. Absorbance was determined at 240 nm (for 30 s) in a spectrophotometer (BioSpec-1601; Shimadzu, Columbia, MD).

### *Cell culture*

Primary cultures of ovine pulmonary arterial endothelial cells (PAECs) were isolated and cultured as previously described (Wedgwood and Black, 2005). The cells were incubated overnight in serum-free Dulbecco's modified Eagle's medium with 1 g/L glucose. In certain studies, cells were preincubated for 18 h with sepiapterin (100 μM) in the presence or absence of the sepiapterin reductase inhibitor N-acetylserotonin (NAS) (100 μM). The cells were then treated for 15 min with $H_2O_2$ and were exposed or not to shear stress for 5 min at 20 dyn/cm$^2$ prior to harvest for LT-PAGE analysis. The cells were harvested by scraping into phosphate-buffered saline and sonicated to disrupt the cellular membrane. Protein was determined using the Bradford assay. PAECs between passages 4 and 6 were used.

### *Shear stress*

Laminar shear stress was applied using a cone-plate viscometer that accepts six-well tissue culture plates, as previously described (Sud *et al.*, 2007). This method achieves laminar flow rates that represent physiological levels of laminar shear stress in the major human arteries, which is in the range of 5–20 dyn/cm$^2$ (Lin *et al.*, 1997), with localized increases to 30–100 dyn/cm$^2$.

### *Detection of $NO_x$*

NO generated by PAECs in response to shear stress was measured using an NO-sensitive electrode with a 2-mm-diameter tip connected to an Apollo 4000 Free-Radical Analyzer (ISO-NOP, WPI, Sarasota, FL), as previously described (Sud *et al.*, 2007).

### *Statistical analysis*

Quantitation of all western blots was performed using a Kodak Image station 440CF and the KDS1D imaging software. The mean ± standard deviation of the densitometric data was calculated. The mean ± standard deviation was also calculated for all eNOS activities. In all cases, comparisons between treatment groups were made using either the unpaired *t*-test or the analysis of variance with posttest Newman–Kuehls using the Prism software program. A $p$-value of $<0.05$ was considered statistically significant.

## Results

### *$H_2O_2$ oxidizes cysteine residues in heNOS to cysteic acid*

To investigate the molecular mechanism by which $H_2O_2$ interacts and inhibits heNOS, we first employed a mass spectroscopic (MS) approach. Cysteine residues can be converted to cysteic acid in the presence of mild oxidizing agents such as $H_2O_2$. This reaction produces a mass shift of 48 Da in peptides containing these modified cysteines. The results from our mass spectra (Table 1) show that the cysteines 94 and 99 (residues involved in the formation of zinc coordination) are oxidized. MS/MS spectrum of the doubly charged ion at $m/z$ 1372.5 was also obtained. The spectrum identifies the oxidation of cysteine 94 to cysteic acid. Similarly, two other peptides confirmed the presence of oxidized cysteines 94 and 99. These peptides appear at $m/z$ 1253.3 (+3) and at $m/z$ 1217.7 (+3) which shows the oxidation of cysteine 99. In addition to the cysteines 94 and 99 residues, we found other oxidized cysteines. Table 1 lists all the peptides containing cysteic acid modifications that were detected

Table 1. List of Digested Peptides of Human Endothelial Nitric Oxide Synthase Showing Mass Shift Due to Formation of Cysteic Acid on Reacting with Hydrogen Peroxide

| *Peptide detected* M, z | *Sequence of the peptide* | *Position of cysteic acid modification* |
|---|---|---|
| 3528.0 Da, 3 | LAAEVHRVLC[a]LERGHMFVC[a]GDVTMATNVLQT | 1104 and 1113 |
| 2791.0 Da, 3 | QAAC[b]ETFC[a]VGEDAKAAARDIFSPKR | 710 |
| 3653.2 Da, 3 | GPC[a]TPRRC[a]LGSLVFPRKLQGRPSPGPPAPEQLLS | 93 and 98 |
| 2512.7 Da, 3 | YRQQDGSVRGDPANVEITELC[a]I | 273 |
| 3493.8 Da, 3 | GTRNLC[a]DPHRYNILEDVAVC[a]MDLDTRTTSS | 367 and 380 |
| 2012.3 Da, 3 | KSVAQEPGPPC[a]GLGLGLGLGL | 14 |
| 3462.9 Da, 3 | LKSVAQEPGPPCGLGLGLGLGLC[a]GKQGPATPAPEPSR | 25 |
| 2563.9 Da, 2 | GPPC[b]GLGLGLGLGLC[a]GKQGPATPAPEP | 25 |
| 3296.9 Da, 3 | QLKPGDPVPC[a]FIRGAPSFRLPPDPSLPCIL | 990 |
| 3760.2 Da, 3 | EVGSITYDTLSAQAQQDGPCTPRRC[a]LGSLVFPRK | 98 |
| 2745.9 Da, 2 | EVGSITYDTLSAQAQQDGPC[a]TPRRC | 93 |

[a]Represents cysteic acid formation (mass shift: 48 Da).
[b]Represents carbamidomethylation (mass shift: 57 Da).

by nano-liquid chromatography–MS/MS (positions of cysteines: 14, 25, 273, 367, 380, 710, 990, 1104, and 1113).

### *Molecular modeling of wild-type heNOS*

Next, we utilized molecular modeling to analyze the effects of cysteic acid modification induced by $H_2O_2$ on the overall quaternary structure of heNOS. The zinc metal is tetrahedrally coordinated by two pairs of symmetrically related cysteine residues from each subunit (Fig. 1A; cysteines 94 and 99). This zinc tetrathiolate metal-binding site is located at the bottom of the dimer interface (Crane *et al.*, 1998; Fischmann *et al.*, 1999). The sulfur atoms in cysteine 94 (from each subunit) have a van der Waals radius of 2.2 Å from the zinc atom. Accordingly, the sulfur atoms of cysteine 99 have a van der Waals radius of 2.4 Å. In addition, the cysteines 94 and 99 are involved in a network of eight H-bonds with the amino acids: L100, two H-bonds of 2.4 Å each with C94; G101, two H-bonds of 2.4 Å each with C99; N466, two H-bonds of 1.7 Å each with C99; and N466, two H-bonds of 2.1 Å each with C99. Based on these molecular modeling measurements, the cysteic acid modification potentially causes the disruption of several crucial H-bonds and four van der Waals interactions that are predicted to lead to drastic quaternary structural changes. These changes would in turn culminate with the collapse of the zinc tetrathiolate metal-binding site, zinc release, and monomerization (Fig. 1B).

### *$H_2O_2$ treatment decreases NO production by dimer collapse*

To test the molecular modeling prediction we initially carried out a series of *in vitro* experiments using purified recombinant heNOS protein. Our model predicts how $H_2O_2$ can inhibit heNOS through a mechanism of dimer collapse mediated, at least in part, by cysteic acid modifications within the tetrathiolate metal-binding site. Based on these predictions, we next evaluated the effect of $H_2O_2$ on heNOS dimer levels. To accomplish this, we initially used LT-PAGE and western blotting analysis and examined the direct oxidation effect of $H_2O_2$ on the dimeric state of heNOS. $H_2O_2$ concentrations in range of hundreds of micromolars have been reported to be generally associated with the consumption of common beverages or smoking (Halliwell *et al.*, 2000). Thus, based on these studies we incubated purified heNOS with pathophysiological concentrations of $H_2O_2$ ranging from 0 to 500 μM. The results obtained demonstrate that $H_2O_2$ induces a concentration-dependent shift in the level of the functional dimeric form to the inactive monomeric form (Fig. 2A, B). Further, gel filtration analysis confirmed that when heNOS was treated with $H_2O_2$ (100 μM) there was complete monomerization of the enzyme (Fig. 2C). Our data show that $H_2O_2$ (100 μM) significantly inhibits heNOS activity as measured by the conversion of [$^3$H]-L-arginine to [$^3$H]-L-citrulline (Fig. 2D).

### *$H_2O_2$ disrupts the zinc tetrathiolate metal-binding site and oxidizes $BH_4$*

To further validate the MS data and the molecular modeling mechanistic prediction, we analyzed the effect of $H_2O_2$ on the integrity of zinc coordination at the dimer interface using the PAR assay. Our results indicate that zinc was released when purified heNOS was exposed to $H_2O_2$ (100 μM), as determined by the increase in absorbance of the PAR-bound zinc emission peak at 500 nm (Fig. 3). These data couple dimer collapse with the disruption of the zinc tetrathiolate metal-binding site. During L-arginine hydroxylation, $BH_4$ acts as a one-electron donor and then it is reduced back to $BH_4$ within eNOS flavoprotein domain, in a calmodulin-dependent manner (Wei *et al.*, 2008). In addition, the $BH_4$ molecule is involved in a H-bonding network that stabilizes the NOS dimer (Raman *et al.*, 1998). Therefore, we next examined the effect induced by $H_2O_2$ on the heNOS cofactor $BH_4$, to further explore the molecular mechanism for the heNOS dimer collapse. Interestingly, when we analyzed the $BH_4$ content of the purified recombinant heNOS after $H_2O_2$ treatment we found it to be predominantly the oxidized $BH_2$ form (Fig. 4). These data suggest that $H_2O_2$ may exert its inhibitory effect on heNOS activity by the simultaneous oxidation of the cysteine residues 94 and 99 and the cofactor $BH_4$. These oxidation events lead to heNOS dimer collapse and diminished rate of L-arginine hydroxylation (one limiting step in the L-arginine/citrulline conversion).

### *Increased $BH_4$ levels prevent dimer collapse and loss of activity*

Dimerization and dimer maintenance appear to be dependent on the presence of zinc, heme, and $BH_4$ cofactors, as

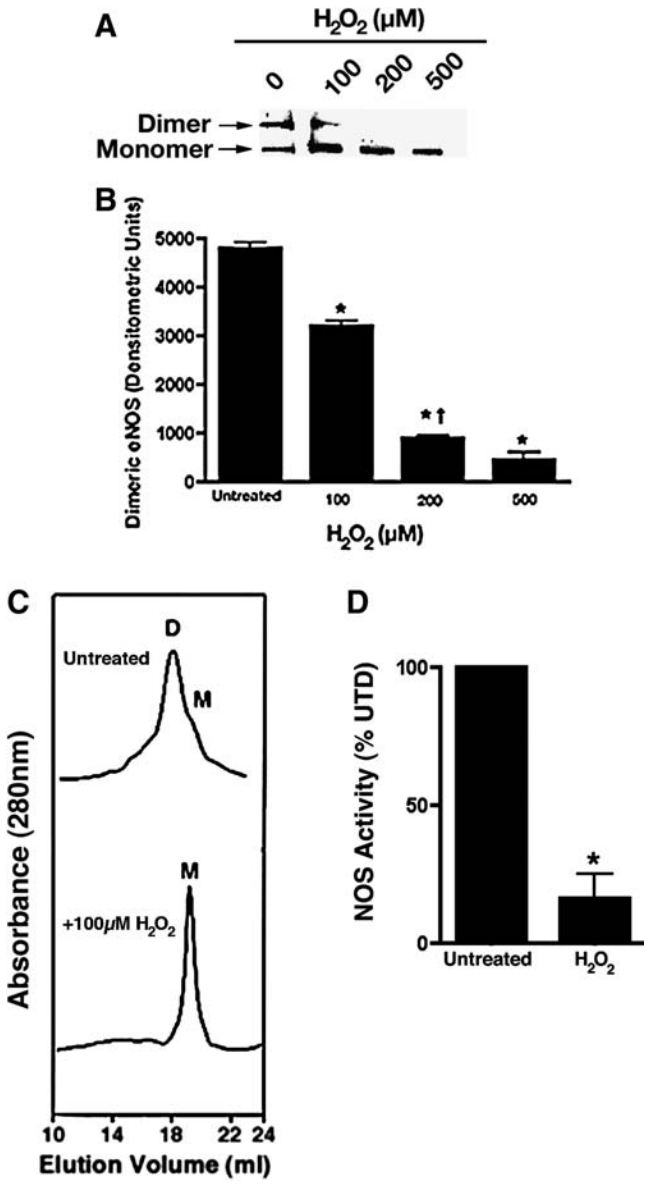


**FIG. 2.** $H_2O_2$-mediated inhibition of purified heNOS *in vitro*. The effect of $H_2O_2$ (0–500 μM) on purified heNOS protein (2 μg) dimer levels were measured using LT-PAGE and western blot analysis. (**A**) A representative western blot is shown demonstrating that $H_2O_2$ dose dependently decreases the level of active heNOS dimers. (**B**) The bar graph shows that the dimeric level of heNOS dimer decreased dose dependently after $H_2O_2$ treatment. Gel filtration analysis of purified heNOS (100 μg) exposed or not to 100 μM of $H_2O_2$ was also carried out to confirm the LT-PAGE data. heNOS is a mixture of dimer and monomer (80:20 ratio); however, $H_2O_2$ treatment induces full monomerization. (**C**) Representative gel filtration chromatograms from three independent experiments. (**D**) The effect of $H_2O_2$ (100 μM) on the ability of heNOS to metabolize [$^3$H]-L-arginine to [$^3$H]-L-citrulline was also determined. The presence of $H_2O_2$ in the reaction mixture results in a 60% inhibition in NOS activity. Values are mean ± SD from three experiments. $^*p < 0.05$ versus untreated, $^\dagger p < 0.05$ versus previous concentration of $H_2O_2$. $H_2O_2$, hydrogen peroxide; LT-PAGE, low-temperature polyacrylamide gel electrophoresis; SD, standard deviation.

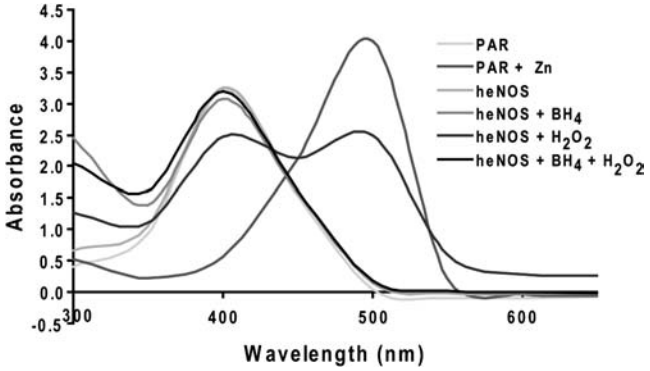


**FIG. 3.** $H_2O_2$ induces release of zinc from heNOS. Purified heNOS (1 mg) was treated with and without $H_2O_2$ (100 μM) in the presence or absence of $BH_4$ (100 μM) for 30 min at 37°C (in the dark) in a cuvette containing PAR (150 μM). A cuvette containing only heNOS was used to autozero the spectrophotometer. Absorbance scan spectra were recorded between 300 and 600 nm. Shown is a representative recording from three independent experiments. $H_2O_2$ causes a release of zinc from the heNOS dimer that was prevented by the presence of excess $BH_4$. $BH_4$, tetrahydrobiopterin; PAR, 4-(2-pyridyl (azo) resorcinol).

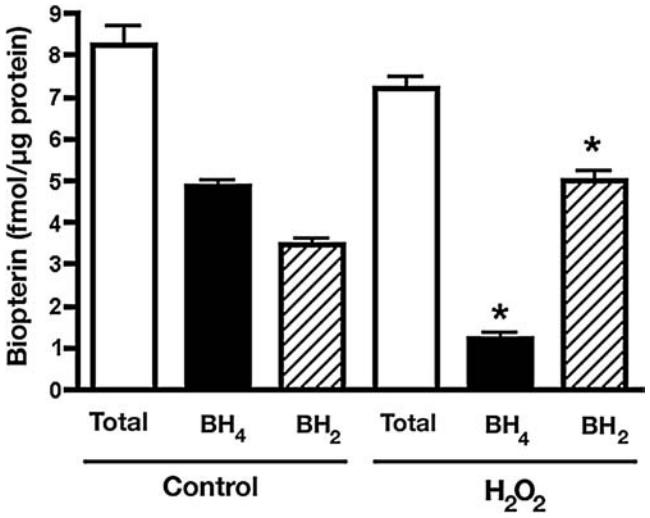


**FIG. 4.** $H_2O_2$ exposure oxidizes bound $BH_4$ in recombinant heNOS. DTT-free pure heNOS (100 μg) was incubated with $BH_4$ (50 μM), unbound $BH_4$ was removed, and heNOS was treated with $H_2O_2$ (10 μM) at 37°C for 30 min. The levels of total $BH_4$ and $BH_2$ bound to the protein were determined. Results were expressed as fmol/μg protein ± SD. $n = 3$. $^*p < 0.05$ versus untreated.

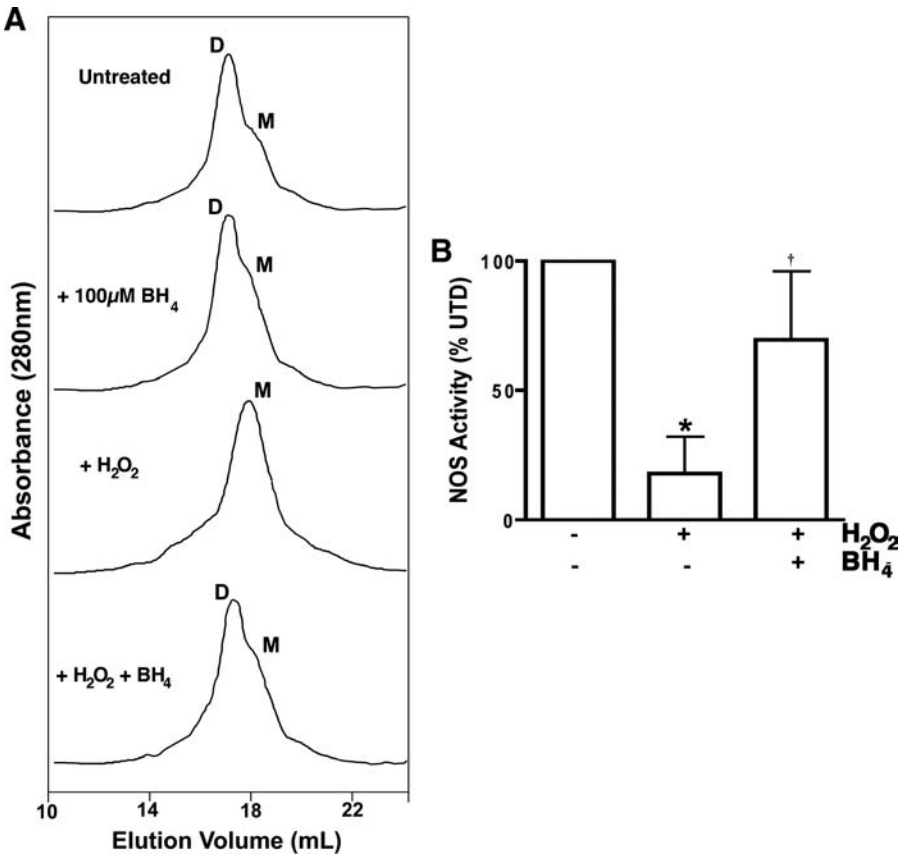


**FIG. 5.** Increasing $BH_4$ levels decreases the $H_2O_2$-mediated heNOS dimer collapse. (**A**) Representative gel filtration chromatograms from three independent experiments. (**B**) The presence of $BH_4$ prevents dimer collapse induced by $H_2O_2$. $BH_4$ also attenuates the $H_2O_2$-mediated inhibition of [$^3$H]-L-arginine to [$^3$H]-L-citrulline conversion by heNOS. Values are mean ± SD from three experiments. $^*p < 0.05$ versus untreated, $^\dagger p < 0.05$ versus no additional $BH_4$.

well the substrate L-arginine. Therefore, we next preincubated purified heNOS with $BH_4$, followed by treatment with the highest pathophysiological concentration of $H_2O_2$, to determine whether increasing $BH_4$ levels could prevent the heNOS dimer collapse induced by $H_2O_2$. We then analyzed the protein samples by gel filtration chromatography. These gel filtration data suggest that purified WT heNOS exists as a mixture of dimeric (80%) and monomeric (20%) forms, and the enzyme shifts completely to the monomeric inactive form after $H_2O_2$ exposure (Fig. 5A). $BH_4$ had no effect on heNOS dimer levels in the absence of $H_2O_2$ (Fig. 5A). However, preincubation with excess $BH_4$ (100 μM) protects the dimer levels from $H_2O_2$-induced collapse (Fig. 5A). heNOS activity was measured in the presence and absence of $BH_4$ and $H_2O_2$. Our results indicate that preincubation of purified heNOS with $BH_4$ significantly preserved heNOS activity after challenge by $H_2O_2$ (Fig. 5B). To further understand the role of $BH_4$ in heNOS activity maintenance during acute oxidative stress induced by $H_2O_2$, we measured $H_2O_2$ dismutation in the presence of $BH_4$. Interestingly, we found that $BH_4$ acts as a catalase mimetic by stimulating the conversion of $H_2O_2$ to $H_2O$ by 15-fold (Fig. 6). These data suggest that the $BH_4$ may exert a dimmer-stabilizing effect due to its antioxidant capacity.

Finally, we determined whether disruption of the eNOS dimer could be induced by increased levels of $H_2O_2$ in cultured PAECs. PAECs were exposed to $H_2O_2$ (100 μM) and

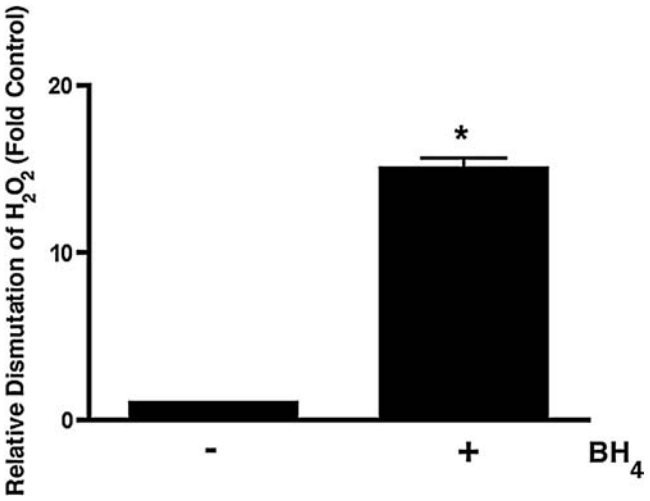


**FIG. 6.** $BH_4$ acts as a catalase mimetic. A 10 mM $H_2O_2$ in 50 mM potassium phosphate buffer (pH 7.8) was incubated in the presence or absence of $BH_4$ (14 μM) and the rate of conversion of $H_2O_2$ to $H_2O$ was determined spectrophotometrically at 240 nm (for 30 s). Data are represented as relative changes from spontaneous $H_2O_2$ to $H_2O$ conversion; $n = 3$. $^*p < 0.05$ versus no $BH_4$.

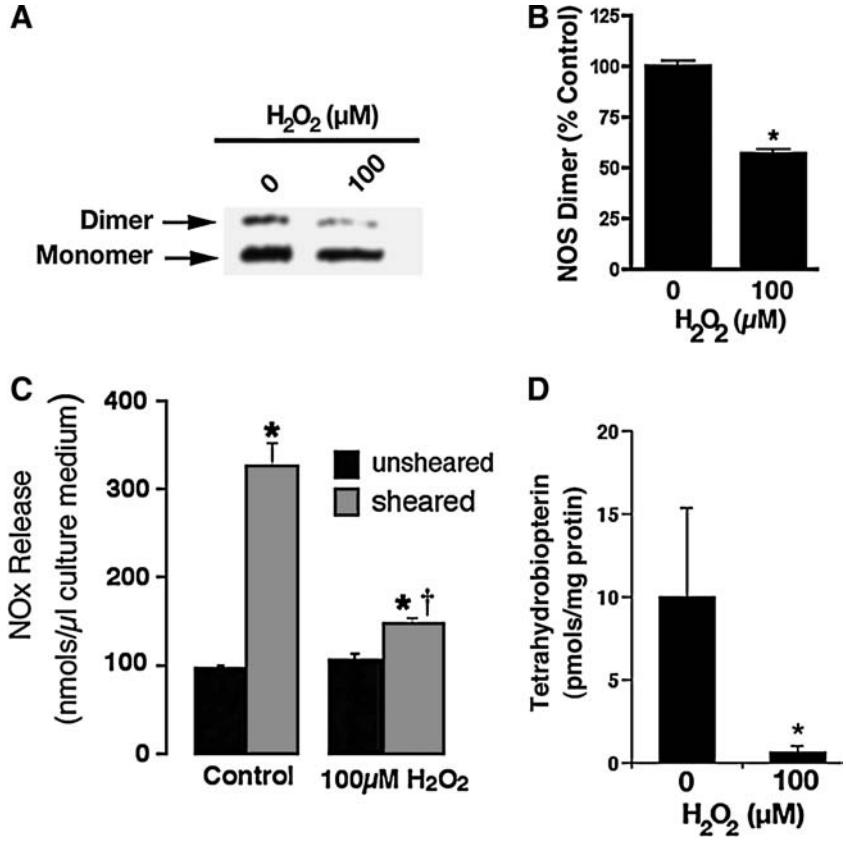


**FIG. 7.** $H_2O_2$ exposure disrupts the eNOS dimer in ovine PAECs. PAECs were exposed to $H_2O_2$ (100 μM) for 15 min. Protein extracts were then prepared and separated on 7.5% polyacrylamide gels using LT-PAGE, electrophoretically transferred to Hybond membranes, and analyzed using a specific antiserum raised against eNOS. (**A**) A representative western blot is shown. (**B**) The densitometric values demonstrate that $H_2O_2$ decreases the level of eNOS dimers in PAECs and decreases the NO generation (**C**) in response to laminar shear stress (5 min, 20 dyn/cm$^2$). (**D**) $BH_4$ levels (expressed as pmol/mg protein) are also decreased in cells exposed to $H_2O_2$. Values are mean ± SD; $n = 3$–6. *$p < 0.05$ versus untreated. †$p < 0.05$ versus no $H_2O_2$. PAECs, pulmonary arterial endothelial cells.

then LT-PAGE and western blot analysis were performed to examine the dimeric state of eNOS. The results obtained indicate that there is a significant reduction in the level of dimeric functional eNOS in $H_2O_2$-treated PAECs (Fig. 7A, B) and a reduction in NO generation in response to laminar shear stress indicating a loss of enzyme activity (Fig. 7C). This was also associated with a reduction in cellular $BH_4$ levels (Fig. 7D). Further, we found that if PAECs were preincubated with the $BH_4$ precursor sepiapterin, the eNOS dimer was protected against $H_2O_2$ challenge (Fig. 8 A, B), and that NO generation was preserved when cells were exposed to laminar shear stress (Fig. 8C).

## Discussion

NOS subunit dimerization serves as a point of biochemical regulation (Ratovitski *et al.*, 1999) and data from Stuehr's group indicated that NOS dimerization could be a potential target for selective control through pharmacologic intervention (Sennequier *et al.*, 1999; Panda *et al.*, 2002). To catalyze NO formation, eNOS must assemble into a homodimeric form (Rodriguez-Crespo *et al.*, 1996). However, it is still not well understood how NOS isoforms dimerize. This is due, at least in part, to the fact that the complete crystal structure has not been determined for any NOS isoform. Consequently, the complete dimer interface of eNOS remains to be elucidated and neither the dimerization of NOS proteins nor the mechanisms that control the dimer/monomer shift have been completely elucidated. One possible way of controlling dimer/monomer shift is through oxidation of cysteine residues that are located at dimer interfaces to cysteic acid. Cysteic acid modifications are a not uncommon modification because an increasing number of proteins have been shown to be a target for $H_2O_2$-induced cysteine–cysteic acid posttranslational modification. The list of target proteins include human apoprotein B-100, peroxiredoxins, promatrix metalloproteinases, nitrile hydratases, tubulin, vimentin, phophoglycerate kinase 1, ATP synthase®, enolase nucleophosmin, heat-shock cognate 54-kDa protein, peroxiredoxin I, glyceraldehyde 3-phosphate, and hemoglobin $HbA_o$ (Murakami *et al.*, 2000; Fu *et al.*, 2001; Rabilloud *et al.*, 2002; Paron *et al.*, 2004; Jia *et al.*, 2007). In addition, the data presented here describe, for the first time, the presence of 11 cysteines within the heNOS sequence that are susceptible to oxidation to cysteic acid after micromolar $H_2O_2$ treatment (Table 1). The mass spectra analyses show that both exposed cysteines 94 and 99 are oxidized (Table 1). $H_2O_2$ can directly oxidize proteins especially if the $pK_a$ of the reactive cysteine is near the acidic range. The local

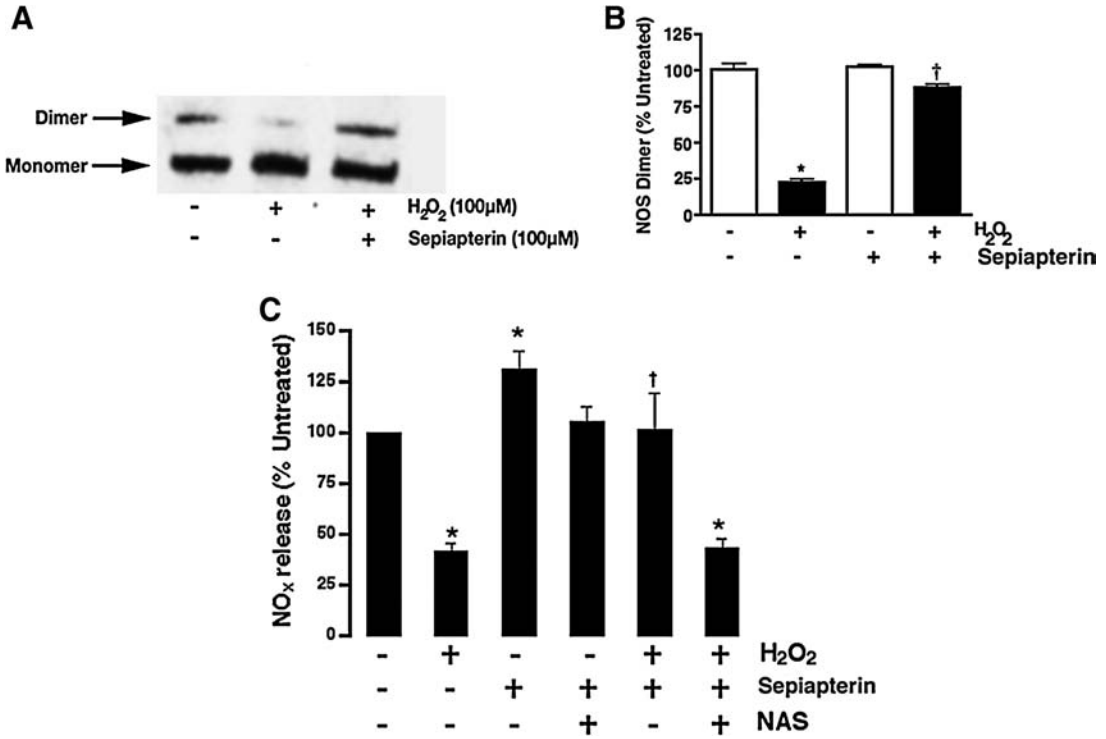


**FIG. 8.** Increasing $BH_4$ levels decrease $H_2O_2$-mediated reduction in eNOS activity in ovine PAECs. PAECs were treated or not with the $BH_4$ precursor sepiapterin (100 μM) for 18 h and then exposed to $H_2O_2$ (100 μM) for 15 min. Protein extracts were then prepared and separated on 7.5% polyacrylamide gels via LT-PAGE, then electrophoretically transferred to Hybond membranes, and analyzed using a specific antiserum raised against eNOS. (**A**) A representative western blot is shown. (**B**) The densitometric values demonstrate that $BH_4$ reduces the $H_2O_2$-mediated decrease in eNOS dimers. Cells were also treated or not with the $BH_4$ precursor sepiapterin (100 μM) for 18 h in the presence or absence of N-acetylserotonin (NAS) (10 μM). Cells were then treated with $H_2O_2$ (100 μM) for 15 min and then exposed to laminar shear stress (20 dyn/cm$^2$) for 5 min. Results are presented as a percentage of $NO_x$ release from sheared cells not exposed to $H_2O_2$ or sepiapterin. Addition of sepiapterin increases NO production by PAECs both in the presence and absence of $H_2O_2$ (**C**). Data are mean ± SD; $n = 6$. *$p < 0.05$ versus sheared alone, $^{\dagger}p < 0.05$ versus $H_2O_2$ alone.

milieu including neighboring amino acids and the binding to metal moieties play a role in maintaining lower p$K_a$ of cysteine, making it more susceptible to oxidants. The zinc tetrathiolate cysteine in eNOS has a low p$K_a$. Thus, this may explain why the tetrathiolate zinc can be directly oxidized by $H_2O_2$. The crystal structure of the heme domain of heNOS has a zinc ion that is tetrahedrally coordinated to two pairs of symmetry-related cysteine residues (corresponding to cysteines 94 and 99 from each monomer), located at the bottom of the dimer interface (Crane *et al.*, 1998; Fischmann *et al.*, 1999). Moreover, cysteine 99 was found to be S-nitrosylated, implicating both cysteine 99 and S-nitrosylation in the regulation of eNOS dimerization and activity (Taldone *et al.*, 2005). Another study from our group links the inhibitory action of NO with the collapse of the zinc tetrathiolate metal-binding site that maintains and stabilizes the dimeric interface (Ravi *et al.*, 2004). More recently, we have identified all the potential cysteine S-nitrosylation sites in heNOS, with 95% of protein coverage by mass spectrometry analysis (Tummala *et al.*, 2008). Based on all these data, we suggest that the molecular mechanism by which $H_2O_2$ exerts its inhibitory effect on heNOS involves, at least in part, the oxidation of cysteine residues 94 and 99 within the zinc coordination. In addition, the MS data show that several other cysteine residues are capable of undergoing cysteic acid modification after $H_2O_2$ treatment. Cysteines 14 and 25, located at the extreme N-terminus of heNOS, can be palmitoylated, thereby targeting eNOS from the golgi apparatus to the plasma membrane where it resides partially in caveolae. Cysteines 367 and 380, residues that were predicted to be located within the HSP90 binding site on heNOS, are also a target for $H_2O_2$ oxidation. Moreover, the cysteine residue 710, located at the flavin mononucleotide (FMN) binding site, is yet another target for $H_2O_2$ oxidation. Also, we identified cysteine residues 990, 1104, and 1113 as being susceptible to oxidation by $H_2O_2$. These cysteines are located in regions of heNOS that have not been implicated in any known biochemical function. Together, these data suggest that $H_2O_2$ may regulate heNOS function in many different ways in addition to inducing dimer collapse through zinc tetrathiolate metal-binding site destruction. Recently, we have identified the cysteine residues that are targets for S-nitrosylation within heNOS (Tummala *et al.*, 2008). Interestingly, the cysteines residues 14, 25, 94, 99, 990, and 1113 are targets for S-nitrosylation and also to cysteic acid modification. These results indicate that heNOS activity can be inhibited in conditions of high oxidative and nitrosative stress, through the modification of the same target cysteines. Moreover, it has been shown that peroxinitrite can disrupt the eNOS zinc metal-binding site through oxidation of the tetrathiolate cysteines 94 and 99 (Zou *et al.*, 2002). And, most re-

cently, Xu *et al.* (2006) demonstrated that hypochlorous acid treatment lead to zinc release by eNOS. Based on these data we now suggest that eNOS monomerization can be considered as a general inhibitory mechanism in response to oxidative and nitrosative stress. It is also worth noting that we have minor discrepancies in our data evaluating eNOS dimer levels using LT-PAGE in conjunction with western blotting and gel filtration. Although gel filtration analysis indicated total dimer collapse, we could still detect some residual eNOS dimer using western blotting. This is likely due to the fact that western blotting is a much more sensitive method compared with gel filtration. In general, antibodies are capable of detecting pico- to femtogram quantities of protein, and thus, even though the dimer amount in western blotting is very low, it will be detected. Conversely, dimer detection using gel filtration is based on absorbance at 280 nm and is therefore less sensitive.

Based on the distance criteria of 2.5 Å for a true H-bond, we built a three-dimensional model of the zinc tetrathiolate cluster. Our model predicts that the zinc coordination is maintained by four symmetrical intramolecular van der Waals interactions between the cysteines 94 and 99. These intramolecular forces hold the zinc atom in the tetrahedral atomic configuration. Additionally, a network of H-bonds between cysteines 94 and 99 and residues L100, G101, and N466 guarantees perfect symmetrical configuration of these cysteines within the zinc coordination. Figure 1B illustrates the molecular modeling prediction of the effects caused by cysteic acid formation within the zinc metal-binding site. The zinc coordination is destroyed in the presence of $H_2O_2$. Cysteine 99 from both chains on the heNOS dimer has a H-bond distance of 2.37 Å from G101. Consequently, serine 102 from both chains relies on the integrity of zinc coordination to be in perfect H-bond distance from the $BH_4$ pocket. Thus, we cannot rule out the possibility that cysteic acid modification of cysteines 94 and 99 may also alter the $BH_4$-binding pocket leading to decreased $BH_4$, L-arginine affinity, and/or heme distortion/loss and further studies will be required to test these possibilities.

Confirming the MS data and the molecular modeling predictions, our *in vitro* activity assay data show that $H_2O_2$ inhibits the L-arginine to citrulline conversion by heNOS. Moreover, the inhibition of heNOS activity by $H_2O_2$ correlates with dimer collapse and loss of zinc from the enzyme. However, there is a contradiction in the literature regarding zinc binding: Some reports have suggested that an intact zinc tetrathiolate metal-binding site is not obligatory for NOS dimerization (Rodriguez-Crespo *et al.*, 1997; Martasek *et al.*, 1998; Ghosh *et al.*, 1999). In addition, Adak *et al.* (2002) have generated a NOS mutant lacking the N-terminal zinc-binding sequence, and interestingly, the enzyme was dimeric. Conversely, it has been suggested that an intact zinc tetrathiolate metal-binding site is essential for formation of sodium dodecyl sulfate (SDS)-resistant NOS dimers but is not essential for catalysis (Hemmens *et al.*, 2000). In addition, it has been shown that zinc content is influenced by cellular pterin levels and that zinc plays a structural, rather than a catalytic, role in maintaining enzymatically active constitutive NOS (Miller *et al.*, 1999). However, Ravi *et al.* (2004) have demonstrated that S-nitrosylation of cysteines 94/99 leads to the disruption of zinc coordination, heNOS monomerization, and activity loss. Based on these data and our modeling predictions, we propose that the molecular mechanism by which $H_2O_2$ induces zinc release involves the oxidation of the tetrathiolate cysteines 94 and 99, and consequently the disruption of van der Waals interactions at the bottom of the dimer interface. Further, our studies in cultured PAECs confirmed that $H_2O_2$ challenge could also induce eNOS dimer collapse and a decrease in NOS activity, indicating that the data generated using recombinant heNOS are not limited to an *in vitro* situation.

Previous studies have indicated that $BH_4$ is involved in an extensive H-bond network which stabilizes the eNOS dimer (Raman *et al.*, 1998), whereas our HPLC analysis data demonstrated that after challenge with a pathophysiological concentration $H_2O_2$ the predominant pterin form bound to heNOS is $BH_2$. Thus, it is possible that if $BH_4$ stabilizes the heNOS dimer, oxidation of $BH_4$ could in turn lead to the distortion of the $BH_4$-binding pocket and consequently helping to promote dimer collapse. Interestingly, $BH_4$ supplementation does protect heNOS dimer against $H_2O_2$ attack both *in vitro* and *in vivo*. However, pterins, such as $BH_4$, have been shown to have antioxidant activity (Kurobane *et al.*, 1995) and we found that the action of $BH_4$ resembles that of a catalase mimetic. Therefore, we suggest that $BH_4$ can protect heNOS dimer disruption by its intrinsic antioxidant capacity that prevents the oxidation of the tetrathiolate cysteines 94/99 rather than through a direct effect on stabilizing the eNOS dimer itself. Indeed, recombinant enzyme expression experiments (Tzeng *et al.*, 1995; Reif *et al.*, 1999) and endothelial cell culture studies (Cai *et al.*, 2002) have found that $BH_4$ promotes eNOS dimerization, protein stability, and NO synthesis. Thus, $BH_4$ appears to have independent, but complementary, roles in regulating eNOS activity. $BH_4$ may be involved in the direct physical stabilization of heNOS in its active dimeric form while also participating in catalytic activity by donating electrons to the ferrous–dioxygen complex in the oxygenase domain as the initiating step of the L-arginine to citrulline conversion (Wei *et al.*, 2008). Finally, $BH_4$, because of its intrinsic antioxidant capacity (catalase mimetic), can protect the cysteines 94 and 99 by preventing their oxidation upon an acute oxidative stress.

Together, our results delineate the molecular mechanism by which $H_2O_2$ promotes dimer collapse and activity loss. This mechanism implicates both oxidation of the cysteines 94 and 99 to cysteic acid within the zinc tetrathiolate metal-binding site and the oxidation of $BH_4$. We further speculate that dimer collapse may be an important regulatory mechanism under conditions of acute oxidative stress where NO bioavailability is decreased.

## Acknowledgments

This research was supported in part by grants HL60190 (to S.M.B.), HL67841 (to S.M.B.), HL72123 (to S.M.B.), and HL70061 (to S.M.B.) from the National Institutes of Health and by a grant from the Fondation Leducq (to S.M.B.). Fabio Vasconcelos Fonseca was supported in part by the NIH training grant 5T32HL06699, and Dean A. Wiseman was supported in part by the grant F32HL090198.

## Disclosure Statement

No competing financial interests exist.

## References


Adak, S., Bilwes, A.M., Panda, K., Hosfield, D., Aulak, K.S., McDonald, J.F., Tainer, J.A., Getzoff, E.D., Crane, B.R., and Stuehr, D.J. (2002). Cloning, expression, and characterization of a nitric oxide synthase protein from *Deinococcus radiodurans*. Proc Natl Acad Sci USA **99,** 107–112.

Aebi, H. (1984). Catalase *in vitro*. Methods Enzymol **105,** 121–126.

Black, S.M., Heidersbach, R.S., McMullan, D.M., Bekker, J.M., Johengen, M.J., and Fineman, J.R. (1999). Inhaled nitric oxide inhibits NOS activity in lambs: potential mechanism for rebound pulmonary hypertension. Am J Physiol **277,** H1849–H1856.

Brennan, L.A., Steinhorn, R.H., Wedgwood, S., Mata-Greenwood, E., Roark, E.A., Russell, J.A., and Black, S.M. (2003). Increased superoxide generation is associated with pulmonary hypertension in fetal lambs: a role for NADPH oxidase. Circ Res **92,** 683–691.

Cai, S., Alp, N.J., McDonald, D., Smith, I., Kay, J., Canevari, L., Heales, S., and Channon, K.M. (2002). GTP cyclohydrolase I gene transfer augments intracellular tetrahydrobiopterin in human endothelial cells: effects on nitric oxide synthase activity, protein levels and dimerisation. Cardiovasc Res **55,** 838–849.

Crane, B.R., Arvai, A.S., Ghosh, D.K., Wu, C., Getzoff, E.D., Stuehr, D.J., and Tainer, J.A. (1998). Structure of nitric oxide synthase oxygenase dimer with pterin and substrate. Science **279,** 2121–2126.

Fischmann, T.O., Hruza, A., Niu, X.D., Fossetta, J.D., Lunn, C.A., Dolphin, E., Prongay, A.J., Reichert, P., Lundell, D.J., Narula, S.K., and Weber, P.C. (1999). Structural characterization of nitric oxide synthase isoforms reveals striking active-site conservation. Nat Struct Biol **6,** 233–242.

Forman, H.J., Fukuto, J.M., and Torres, M. (2004). Redox signaling: thiol chemistry defines which reactive oxygen and nitrogen species can act as second messengers. Am J Physiol Cell Physiol **287,** C246–C256.

Fu, X., Kassim, S.Y., Parks, W.C., and Heinecke, J.W. (2001). Hypochlorous acid oxygenates the cysteine switch domain of pro-matrilysin (MMP-7). A mechanism for matrix metalloproteinase activation and atherosclerotic plaque rupture by myeloperoxidase. J Biol Chem **276,** 41279–41287.

Fukushima, T., and Nixon, J.C. (1980). Chromatographic analysis of pteridines. Methods Enzymol **66,** 429–436.

Ghosh, D.K., Crane, B.R., Ghosh, S., Wolan, D., Gachhui, R., Crooks, C., Presta, A., Tainer, J.A., Getzoff, E.D., and Stuehr, D.J. (1999). Inducible nitric oxide synthase: role of the N-terminal beta-hairpin hook and pterin-binding segment in dimerization and tetrahydrobiopterin interaction. EMBO J **18,** 6260–6270.

Giorgio, M., Trinei, M., Migliaccio, E., and Pelicci, P.G. (2007). Hydrogen peroxide: a metabolic by-product or a common mediator of ageing signals? Nat Rev Mol Cell Biol **8,** 722–728.

Griendling, K.K., Sorescu, D., Lassegue, B., and Ushio-Fukai, M. (2000a). Modulation of protein kinase activity and gene expression by reactive oxygen species and their role in vascular physiology and pathophysiology. Arterioscler Thromb Vasc Biol **20,** 2175–2183.

Griendling, K.K., Sorescu, D., and Ushio-Fukai, M. (2000b). NAD(P)H oxidase: role in cardiovascular biology and disease. Circ Res **86,** 494–501.

Halliwell, B., Clement, M.V., Ramalingam, J., and Long, L.H. (2000). Hydrogen peroxide. Ubiquitous in cell culture and *in vivo*? IUBMB Life **50,** 251–257.

Hallmark, O.G., Phung, Y.T., and Black, S.M. (1999). Chimeric forms of neuronal nitric oxide synthase identify different regions of the reductase domain that are essential for dimerization and activity. DNA Cell Biol **18,** 397–407.

Hemmens, B., Goessler, W., Schmidt, K., and Mayer, B. (2000). Role of bound zinc in dimer stabilization but not enzyme activity of neuronal nitric-oxide synthase. J Biol Chem **275,** 35786–35791.

Hevel, J.M., and Marletta, M.A. (1994). Nitric-oxide synthase assays. Methods Enzymol **233,** 250–258.

Jia, Y., Buehler, P.W., Boykins, R.A., Venable, R.M., and Alayash, A.I. (2007). Structural basis of peroxide-mediated changes in human hemoglobin: a novel oxidative pathway. J Biol Chem **282,** 4894–4907.

Klatt, P., Schmidt, K., Lehner, D., Glatter, O., Bachinger, H.P., and Mayer, B. (1995). Structural analysis of porcine brain nitric oxide synthase reveals a role for tetrahydrobiopterin and L-arginine in the formation of an SDS-resistant dimer. EMBO J **14,** 3687–3695.

Knowles, R.G. (1996). Nitric oxide synthases. Biochem Soc Trans **24,** 875–878.

Kurobane, T., Kojima, S., Yoshimura, M., Icho, T., Kajiwara, Y., and Kubota, K. (1995). Effect of 5,6,7,8-tetrahydroneopterin on the bovine endothelial cell injury induced by cumene hydroperoxide. Jpn J Pharmacol **68,** 263–269.

Lin, M.C., Almus-Jacobs, F., Chen, H.H., Parry, G.C., Mackman, N., Shyy, J.Y., and Chien, S. (1997). Shear stress induction of the tissue factor gene. J Clin Investig **99,** 737–744.

Lubos, E., Handy, D.E., and Loscalzo, J. (2008). Role of oxidative stress and nitric oxide in atherothrombosis. Front Biosci **13,** 5323–5344.

Martasek, P., Miller, R.T., Liu, Q., Roman, L.J., Salerno, J.C., Migita, C.T., Raman, C.S., Gross, S.S., Ikeda-Saito, M., and Masters, B.S. (1998). The C331A mutant of neuronal nitric-oxide synthase is defective in arginine binding. J Biol Chem **273,** 34799–34805.

Miller, R.T., Martasek, P., Raman, C.S., and Masters, B.S. (1999). Zinc content of *Escherichia coli*-expressed constitutive isoforms of nitric-oxide synthase. Enzymatic activity and effect of pterin. J Biol Chem **274,** 14537–14540.

Munzel, T., Sinning, C., Post, F., Warnholtz, A., and Schulz, E. (2008). Pathophysiology, diagnosis and prognostic implications of endothelial dysfunction. Ann Med **40,** 180–196.

Murakami, T., Nojiri, M., Nakayama, H., Odaka, M., Yohda, M., Dohmae, N., Takio, K., Nagamune, T., and Endo, I. (2000). Post-translational modification is essential for catalytic activity of nitrile hydratase. Protein Sci **9,** 1024–1030.

Panda, K., Rosenfeld, R.J., Ghosh, S., Meade, A.L., Getzoff, E.D., and Stuehr, D.J. (2002). Distinct dimer interaction and regulation in nitric-oxide synthase types I, II, and III. J Biol Chem **277,** 31020–31030.

Paron, I., D'Elia, A., D'Ambrosio, C., Scaloni, A., D'Aurizio, F., Prescott, A., Damante, G., and Tell, G. (2004). A proteomic approach to identify early molecular targets of oxidative stress in human epithelial lens cells. Biochem J **378,** 929–937.

Rabilloud, T., Heller, M., Gasnier, F., Luche, S., Rey, C., Aebersold, R., Benahmed, M., Louisot, P., and Lunardi, J. (2002). Proteomics analysis of cellular response to oxidative stress. Evidence for *in vivo* overoxidation of peroxiredoxins at their active site. J Biol Chem **277,** 19396–19401.

Raman, C.S., Li, H., Martasek, P., Kral, V., Masters, B.S., and Poulos, T.L. (1998). Crystal structure of constitutive endothelial nitric oxide synthase: a paradigm for pterin function involving a novel metal center. Cell **95,** 939–950.

Ratovitski, E.A., Bao, C., Quick, R.A., McMillan, A., Kozlovsky, C., and Lowenstein, C.J. (1999). An inducible nitric-oxide

synthase (NOS)-associated protein inhibits NOS dimerization and activity. J Biol Chem **274,** 30250–30257.

Ravi, K., Brennan, L.A., Levic, S., Ross, P.A., and Black, S.M. (2004). S-nitrosylation of endothelial nitric oxide synthase is associated with monomerization and decreased enzyme activity. Proc Natl Acad Sci USA **101,** 2619–2624.

Reif, A., Frohlich, L.G., Kotsonis, P., Frey, A., Bommel, H.M., Wink, D.A., Pfleiderer, W., and Schmidt, H.H. (1999). Tetrahydrobiopterin inhibits monomerization and is consumed during catalysis in neuronal NO synthase. J Biol Chem **274,** 24921–24929.

Rodriguez-Crespo, I., Gerber, N.C., and Ortiz de Montellano, P.R. (1996). Endothelial nitric-oxide synthase. Expression in *Escherichia coli*, spectroscopic characterization, and role of tetrahydrobiopterin in dimer formation. J Biol Chem **271,** 11462–11467.

Rodriguez-Crespo, I., Moenne-Loccoz, P., Loehr, T.M., and Ortiz de Montellano, P.R. (1997). Endothelial nitric oxide synthase: modulations of the distal heme site produced by progressive N-terminal deletions. Biochemistry **36,** 8530–8538.

Sennequier, N., Wolan, D., and Stuehr, D.J. (1999). Antifungal imidazoles block assembly of inducible NO synthase into an active dimer. J Biol Chem **274,** 930–938.

Sheehy, A.M., Burson, M.A., and Black, S.M. (1998). Nitric oxide exposure inhibits endothelial NOS activity but not gene expression: a role for superoxide. Am J Physiol **274,** L833–L841.

Sud, N., Sharma, S., Wiseman, D.A., Harmon, C., Kumar, S., Venema, R.C., Fineman, J.R., and Black, S.M. (2007). Nitric oxide and superoxide generation from endothelial NOS: modulation by HSP90. Am J Physiol Lung Cell Mol Physiol **293,** L1444–L1453.

Taldone, F.S., Tummala, M., Goldstein, E.J., Ryzhov, V., Ravi, K., and Black, S.M. (2005). Studying the S-nitrosylation of model peptides and eNOS protein by mass spectrometry. Nitric Oxide **13,** 176–187.

Tummala, M., Ryzhov, V., Ravi, K., and Black, S.M. (2008). Identification of the cysteine nitrosylation sites in human endothelial nitric oxide synthase. DNA Cell Biol **27,** 25–33.

Tzeng, E., Billiar, T.R., Robbins, P.D., Loftus, M., and Stuehr, D.J. (1995). Expression of human inducible nitric oxide synthase in a tetrahydrobiopterin (H4B)-deficient cell line: H4B promotes assembly of enzyme subunits into an active dimer. Proc Natl Acad Sci USA **92,** 11771–11775.

Wainwright, M.S., Arteaga, E., Finak, R., Ravi, K., Chace, D.H., and Black, S.M. (2005). Loss of nitric oxide synthase (NOS) activity after hypoxia-ischemia in the newborn rat is not associated with a decrease in tetrahydrobiopterin or NOS dimer levels. Brain Res **156,** 183–192.

Wedgwood, S., and Black, S.M. (2005). Endothelin-1 decreases endothelial NOS expression and activity through ETA receptor-mediated generation of hydrogen peroxide. Am J Physiol Lung Cell Mol Physiol **288,** L480–L487.

Wei, C.C., Wang, Z.Q., Tejero, J., Yang, Y.P., Hemann, C., Hille, R., and Stuehr, D.J. (2008). Catalytic reduction of a tetrahydrobiopterin radical within nitric-oxide synthase. J Biol Chem **283,** 11734–11742.

Xu, J., Xie, Z., Reece, R., Pimental, D., and Zou, M.H. (2006). Uncoupling of endothelial nitric oxidase synthase by hypochlorous acid: role of NAD(P)H oxidase-derived superoxide and peroxynitrite. Arterioscler Thromb Vasc Biol **26,** 2688–2695.

Zou, M.H., Shi, C., and Cohen, R.A. (2002). Oxidation of the zinc-thiolate complex and uncoupling of endothelial nitric oxide synthase by peroxynitrite. J Clin Investig **109,** 817–826.

Address correspondence to:
*Stephen M. Black, Ph.D.*
*Vascular Biology Center*
*Medical College of Georgia*
*Augusta, GA 30912*

*E-mail:* sblack@mcg.edu

Received for publication January 14, 2009; received in revised form October 17, 2009; accepted October 19, 2009.